

A study of baroclinic instability in a cylindrical annulus with the temperature gradient imposed on the lower surface

By TIMOTHY L. MILLER¹ AND NATHANIEL D. REYNOLDS²†

¹NASA/Marshall Space Flight Center, Earth Science and Applications Division,
Huntsville, AL 35812, USA

²Mathematical Sciences Department, University of Alabama in Huntsville,
Huntsville, AL 35899, USA

(Received 15 January 1991 and in revised form 30 May 1991)

Laboratory experiments and numerical modelling studies have been performed for a rotating, thermally driven fluid system in a cylindrical annulus with a vertical rotation vector and axis of symmetry. The thermal forcing was through the imposition of an axisymmetric temperature gradient on a thermally conducting lower boundary, with additional heating through the outer sidewall. The upper and inner walls were nominally insulating. Flow patterns were observed in the experiments through the use of small, reflective flakes (Kalliroscope) in the working fluid, which was water. The rotation rate and temperature difference were varied to construct a regime diagram in thermal Rossby number–Taylor number space. The curve separating axisymmetric flow from wave flow is ‘knee-shaped’, similar to the side-heated and -cooled baroclinic annulus which has been extensively investigated previously. Very near the transition curve, the initial wavenumber persists indefinitely, but well into the wave regime the initial wavenumber is higher than the equilibrated value. Far enough into the wave regime, the initial waves have wavenumbers several times that of the equilibrated value, and the initial disturbances form near the outer wall very early in the experiment. Numerical studies indicate that these waves are effective in distributing heat and that they occur in a region of positive static stability. These waves rapidly grow inward to fill the annulus and reduce in number as weaker waves are absorbed by the stronger ones. The period of transition between these waves and the equilibrated long-wave pattern is characterized by irregular flow. Closer to the transition curve, the temporal transition to longer waves as the flow equilibrates is simpler, with initial waves filling the annulus. In that case, the transition is characterized by a slow process of individual waves weakening and merging with adjacent waves.

1. Introduction

The fluid dynamics of a rotating system with horizontal temperature gradients is fundamental to geophysical and astrophysical systems, and there have been many theoretical and experimental studies of such flows performed. Study of flow in a rotating annulus with a temperature difference maintained on the two sidewalls has assisted in validating the theory of baroclinic instability (Barcilon 1964), and it continues to facilitate the study of nonlinear behaviour in a baroclinic fluid (e.g.

† Current affiliation: The Boeing Company, PO Box 240002, Huntsville, AL 35824, USA.

Buzyna, Pfeffer & Kung 1989). While the system with thermally conducting sidewalls (hereafter called the 'conventional' annulus) has been extensively investigated (reviewed by Hide & Mason 1975), the system with a temperature gradient imposed upon thermally conducting horizontal surfaces has been studied relatively little. Miller & Fowles (1986) and Hathaway & Fowles (1986) investigated the flow in a rotating annulus with temperature gradients imposed upon the upper and lower surfaces, while the outer and inner walls were nominally insulating. These experiments resulted in a range of instabilities from baroclinic waves to small-scale convection, including a mix of both types of instabilities which was manifested by large-scale waves with irregular wiggles. Hignett, Ibbetson & Kilworth (1981) studied the flow in a rotating annulus with the gradient imposed upon the lower horizontal surface and with all other surfaces adiabatic. Most of the description of their experimental results dealt with steady axisymmetric flow, there being a brief, qualitative description of baroclinic waves for rapid enough rotation. Hignett *et al.* (1981) did not attempt to determine the full transition curve for baroclinic waves, but apparently studied flow near the 'upper transition', which occurs for large ΔT and for which waves occur for large enough rotation rate (with a fixed ΔT). There were no reports of wavenumbers or flow structure for the baroclinic wave regime. Koschmeider & Lewis (1986) studied the Hadley circulations in a shallow, full cylindrical disk, with a temperature gradient imposed upon the bottom and an isothermal condition on top. The rotation rates in the latter study were apparently too small to permit baroclinic waves to ensue.

A system with the temperature profile imposed on the horizontal surface may be of interest to atmospheric dynamicists because the surface gradient is not pushed by the flow to the sidewalls, as in the conventional annulus. In this sense, it is more like the atmospheric situation which has maximum baroclinicity at or near the lower surface, void of any vertical boundary effects. Furthermore, to be more like the atmosphere in the sense of having more nearly horizontal isotherms, it is desirable to study a system with a vertical height of less than the annulus width. However, in that case the conventional system has a more limited heat-transfer surface. The system with the temperature gradient imposed on both horizontal surfaces has some scientific advantages (see Miller & Fowles 1986), but if it is desired to optically view the flow patterns through the horizontal surface there is a strong practical constraint. The only available transparent, heat-conducting material is synthetic sapphire, the expense of which constrains the size of the annulus to be fairly small. The present authors decided upon a slightly modified version of the configuration used by Hignett *et al.* (1981). The lower surface is a thermal conductor (copper) and the upper lid is a thermal insulator (clear Plexiglas). Besides dimensions, the difference between the current annulus and that of Hignett *et al.* is that the outer wall in the present case is made of a heat-conducting material. Numerical design studies showed that the use of an insulating vertical wall results in short-wave, convective instabilities (some of which were discussed by Hignett *et al.*) in the outer part of the flow cell which complicates the analysis of the longer wavelength modes which are of primary interest. The convective modes are suppressed by the use of a thermally conducting outer wall.

The primary purpose of the present work is to provide a general description of the first-order behaviour of the system – i.e. the fundamental flow regime (axisymmetric or baroclinic wave) and wavenumber in the case of the baroclinic wave regime. For a broad range of parameter space, we describe experimental observations of points of transition between axisymmetric and wave flow, equilibrated wavenumbers for

quasi-steady wave flow, and transient states that occur either prior to equilibrated flows or indefinitely. The transient phenomena studied occur on short timescales, as long-term time behaviour has not been investigated. Also included are descriptions of numerical simulations of the experiments, including some of those aspects mentioned in the preceding sentence. The numerical results complement the laboratory work by allowing detailed study of the flow features and by selectively restricting certain interactions between flow components.

2. Description of the apparatus

The flow cell was constructed of thermally conducting bottom and outer walls, and insulating upper and inner walls. The inner and outer radii were 7.0 and 13.3 cm, respectively, and the depth was 2 cm. In order to decouple the heat flow within the flow cell and that in the solid apparatus containing it, the base of the annulus was constructed from copper of thickness 0.63 cm, and the outer wall was made of copper 3.3 cm thick. The lower surface was electroplated with gold to prevent deterioration of the surface, and the outer wall was coated with flat black enamel paint to avoid scattering of the laser beam (the purpose of which will be described below). The upper lid was made of 1.9 cm thick Plexiglas, and the inner wall was of Plexiglas of thickness 0.63 cm. The temperature profile was imposed by water baths circulating through large annular copper channels which were in firm thermal and mechanical contact under the annulus base and outside the flow cell inner and outer radii, as shown in figure 1(a). The circulating channels were constructed so that each of the water baths made two loops around the annulus in opposite directions for the purpose of maintaining axisymmetry of the boundary temperature field (see figure 1b). The lid had a small hole (diameter ≈ 0.3 cm) near the outer wall for filling the flow cell and to allow for thermal expansion. The hole was filled with a loose-fitting plastic plug to reduce the effects of an open cavity upon the flow during the experiments. Physical constants and their values are given in table 1.

Boundary temperatures near the bottom and outer flow cell surface were measured by means of glass bead thermistors (0.16 cm diameter) which were coated with thermally conducting grease and mounted in the copper through holes drilled in the bottom of the copper plate and in the outside of the outer wall, i.e. from the outside of the flow cell (see figure 1a). The thermistors, which were not in contact with the flow, were about 0.15 cm from the flow cell boundary. There was an array of 16 thermistors in the lower surface and 4 thermistors in the outer wall, the former arranged in groups of 4 thermistors at radii of 7.6 cm, 9.3 cm, 11.0 cm, and 12.7 cm, each group 90° apart longitudinally. The outer thermistors were at the same longitudes as the lower ones and were placed at the top edge of the flow cell. The resistance of each thermistor was measured with an ohmmeter which was precise to better than 0.1% of the resistance of the thermistor, and the temperature was obtained by using a third-degree polynomial derived from a least-squares fit to calibration data which had been taken at 1°C increments for the range of temperatures expected (5° – 35°C). The temperatures thus determined were accurate to a standard deviation of about 0.01°C . The circulating baths controlled the circulating water temperature to within about $\pm 0.01^\circ\text{C}$, with occasional, brief excursions of $\pm 0.02^\circ\text{C}$. Because of the thermal mass of the apparatus, these brief excursions were not felt by the working fluid (confirmed by the thermistor readings). Measurements of the boundary temperatures at various temperature differences confirmed the near axisymmetry of the forcing, which had a non-axisymmetry of less

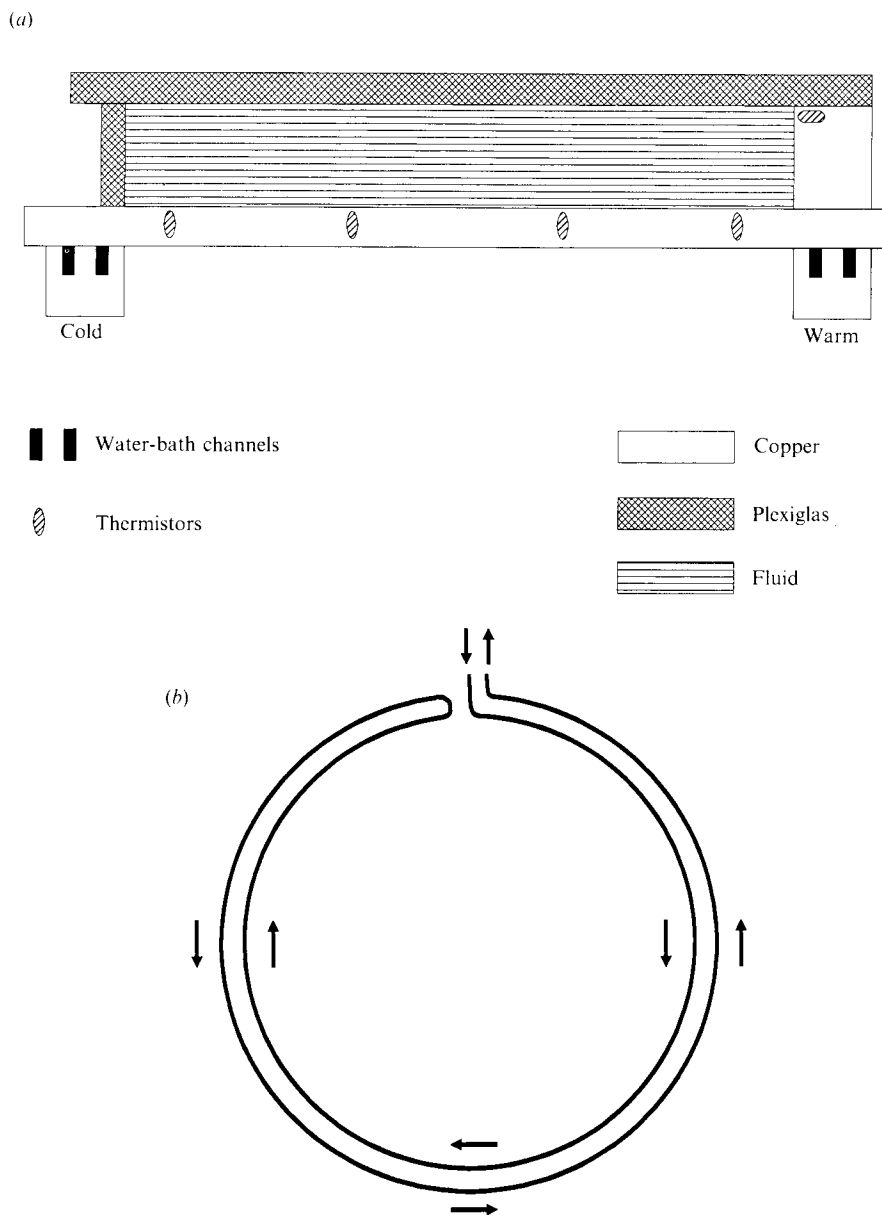


FIGURE 1. Schematic sketches of the flow cell annulus cross-section (a) and the water-bath loop system (b). In part (a), the outer wall is to the right.

g	gravity	980 cm s^{-1}
d	vertical depth of flow cell	2.0 cm
a	inner radius of flow cell	7.0 cm
b	outer radius of flow cell	13.3 cm
α	thermal expansivity	$0.0002054 \text{ (}^\circ\text{C)}^{-1}$
ν	kinematic viscosity	$0.011 \text{ cm}^2 \text{ s}^{-1}$
κ	thermal conductivity	$0.00142 \text{ cm}^2 \text{ s}^{-1}$

TABLE 1. Physical Constants.

than 2% of the imposed temperature difference in the flow cell. The temperature difference across the flow cell (ΔT) was estimated by measuring the temperatures for one group of four thermistors, fitting a logarithmic curve through those four points, and using that curve to extrapolate to the inner and outer radii of the flow cell. The ΔT was about $\frac{5}{8}$ of that of the circulating baths, and the maximum ΔT available was about 16 °C.

The apparatus was centred on a turntable, model 813/404D by Contraves-Goerz Corporation, which was driven by a servo-controlled, permanent-magnet DC motor and had both instantaneous and long-term accuracy (manufacturer's specifications) of 0.1% of the selected rate or 0.1° per s (whichever is larger). The actual rotation rate was not verified independently of the controller supplied with the table. The procedure for ensuring a level apparatus and a vertical rotation axis was to level the turntable top to within about 0.002 rad, and then to level the apparatus to the same accuracy. Lack of wobble in the rotation axis was verified optically through the use of a carefully aligned laser beam from above and a flat mirror sitting on the apparatus (without the Plexiglas lid).

The data obtained (other than thermal boundary conditions) consisted of flow patterns; no velocity or flow temperature data were taken. The patterns were observed through the use of a 0.33% solution of Kalliroscope with deionized water. The Kalliroscope consists of small, reflective flakes which become aligned with shear in the flow. A laser beam (1–4 mm wide) was used to assist in the flow visualization. The laser beam was directed down the axis of symmetry onto a rapidly spinning mirror which was mounted at a 45° angle in the centre of the annulus, thus forming an apparent sheet of light. It was found that the use of the laser greatly enhanced the visualization. (Without the laser, higher concentrations of Kalliroscope are needed.) For the photographs shown here, the laser was centred at a height of about 0.5 cm from the lower surface of the flow cell. For the determination of points of transition from axisymmetric flow to wave flow, an insulating foam was used in the centre, above, and around the sides of the annulus. The foam on top and in the centre was briefly removed to make observations of the flow. It was found that significant differences in the transition points were obtained with and without the foam; when the foam was included, the results were much closer to the numerical predictions (especially near the lower transition). Photographs were taken of many of the wave patterns, and some of the flow pattern evolutions were recorded by video tape.

3. Description of the numerical model

The model is based upon the Navier–Stokes equations and is described in Miller, Lu & Butler (1991) and in an internal report available from the present authors. A brief description of the fundamental aspects of the code is given here. The equations are finite differenced in the axial and radial directions, and Fourier modes ('waves') are used longitudinally. For the terms involving wave–wave interactions, the Fourier transform method is used. That is, the total wave fields are transformed to a longitude grid where the quadratic terms needed for the nonlinear tendencies are calculated. These are then transformed to spectral space, where the tendencies for each wave component are calculated. The meridional grid is stretched to give higher resolution near the boundaries. Centred, conservative spatial differencing is used, which is accurate to second order for an unstretched grid. (Note that flow velocities are not large enough in the present cases to require such methods as upwind differencing.) The computer code permits the calculation of axisymmetric states,

linear waves (based on a previously computed axisymmetric state), single or multiple waves with feedback to the mean state but not between waves, and multiple waves with all interactions included. In the latter case, a wave factor can be used (i.e. the set of waves considered is $n, 2n, 3n, \dots, Nn$, where n and N are positive integers). All Fourier components (including the axisymmetric field) use the same finite-differencing scheme.

The boundary conditions assumed in the calculations are no-slip on all four surfaces, no heat flux on the inner and upper surfaces, and fixed temperature on the outer and lower surfaces. The profile on the lower surface was logarithmic in radius, and the profile on the outer sidewall was linear in height. The vertical temperature difference on the outer wall was taken to be 5% of the radial difference (warmer above), which was approximately equal to that measured by the thermistors in the apparatus.

4. Experimental results

4.1. Transitions between waves and axisymmetric flow

All experiments were begun by first allowing the circulating baths to equilibrate to the desired temperature. (The arithmetic mean temperature of the two baths was always near 21 °C.) An additional half hour (minimum) was allowed to make sure that the apparatus itself had thermally equilibrated. Then, the flow cell was vigorously mixed by a sequence of rapid reversals of rotation which created strong turbulence within the flow cell. The turntable was then immediately set to the desired rotation rate. All results discussed here were obtained by allowing the experimental system and the flow to equilibrate with conditions of constant rotation rate and temperature difference. Well inside the wave regime, it was possible to ascertain that waves were present within a few minutes, but near the transition curve (especially the low transition) it was necessary to wait several hours before concluding whether a given set of imposed conditions yielded an axisymmetric or a wavy state. It should be emphasized that great care was required in thermal condition in order to obtain consistent results, especially near the lower transition. In particular, it was necessary to place foam insulation in the centre and over the sides and top of the apparatus and to wait long enough (*a*) for the apparatus to attain an equilibrated mean temperature before starting the experiment and (*b*) for the flow to equilibrate before ending the experiment. The transition results are summarized in figure 2. It is seen that the transition curve in Taylor number (Ta)–thermal Rossby number (Ro) space is knee-shaped, similar to that of the conventional annulus. For the lower part of the transition curve, the transition points were determined by varying the temperature difference for a fixed rotation rate, and the upper transition points were determined by varying the rotation rate for a fixed temperature difference. Note that the wavenumber observed is a function of the external parameters, with the longer waves ($k \approx 6$) apparent near the upper transition. This behaviour is also observed in the conventional annulus experiments (e.g. Fowles & Hide 1965). Hignett *et al.* (1981) measured a parameter $Q (= 2\Omega(b-a)^{1/2}k^2/g\alpha\Delta T)^{1/2}v^{1/2}$; a measure of the ratio of the thickness of the upper thermal boundary layer to that of the Ekman layer) at the upper transition and obtained a value of 3.4. We obtained the somewhat larger value of 4.0.

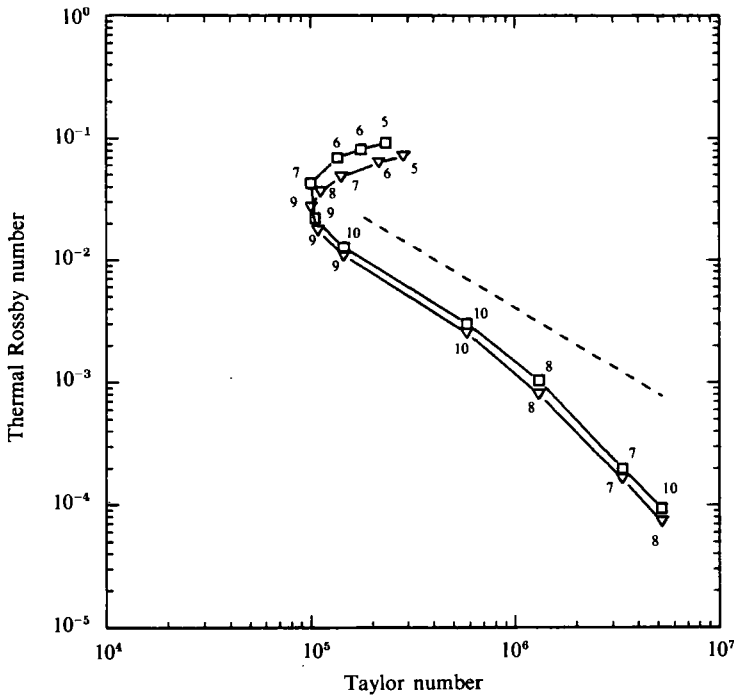


FIGURE 2. Transition curves in thermal Rossby number–Taylor number space. The squares mark transition points determined experimentally, and the triangles are those determined with the numerical model, with the wavenumber shown. For reference, the dashed line represents a horizontal temperature difference of 3 °C; lines of constant rotation rate are vertical (not shown). The definition of thermal Rossby number is: $Ro = g\alpha\Delta Td/4\Omega^2(b-a)^2$; for Taylor number: $Ta = 4\Omega^2d^4/\nu^2$.

4.2. Evolution from short to long waves

Figure 3 shows a summary of the initial (first) and final wavenumbers observed. Near the transition curve, it was observed that the initial wavenumber persisted indefinitely, or in some cases and depending on how close it was to the transition curve, there was a transition to a wave pattern with fewer lobes. This transition would occur by one of the lobes becoming weak and eventually decaying completely, with the other lobes eventually moving around to fill the annulus with uniform spacing. Further from the transition curve, there were cases of further transitions to longer waves, similar to that just described, so that the equilibrated wavenumber was more than one less than that of the initial wave. In the cases where the initial waves filled the annulus width and the transition to fewer waves was due to the sequential loss of individual waves, the initial wavenumber was at most about 20.

Well within the wave regime it was observed that the first asymmetries were smaller-scale waves (wavenumber typically 30–40) which developed very quickly (within a few minutes) and were initially confined to a region near the outer wall. An example of this pattern is shown in figure 4(a). These small waves gradually (and non-uniformly) spread inward to fill the annulus width and reduce somewhat in number (the waves slowest to spread inward were generally consumed by the others), and a large-wave pattern would eventually become dominant (figure 4b). However, the observers were not able to track particular short waves that survived and eventually become long waves. Instead, after the short waves filled the annulus, there was a transition period of irregular flow which gave way to a large-wave pattern.

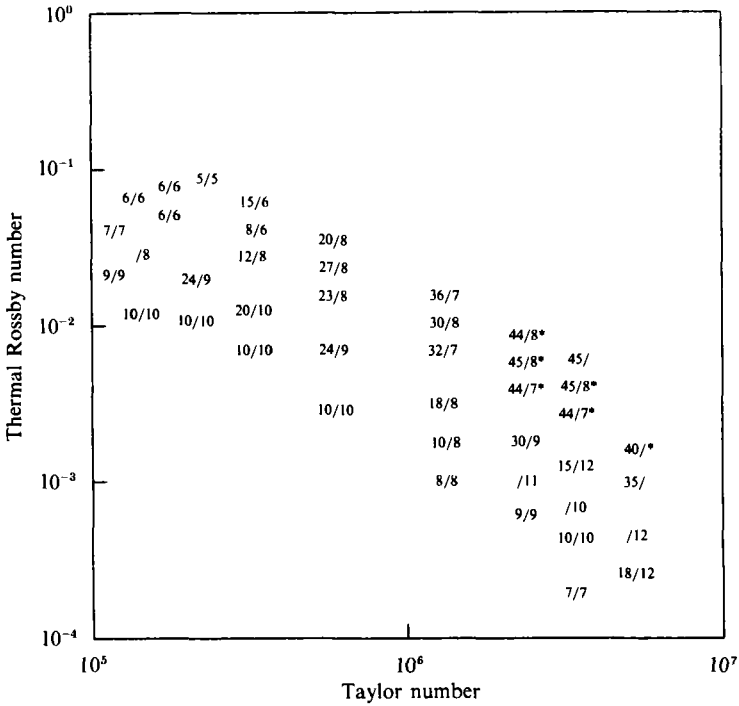


FIGURE 3. Summaries of observed initial/equilibrated ('final') wavenumbers in the laboratory experiments. An asterisk after a number indicates that it is approximate and that the flow is irregular. An asterisk alone indicates that the flow was irregular and the wavenumber was indeterminate.

4.3. Structure of the equilibrated waves

A general description and photographs of some of the equilibrated wave structures (horizontal planforms) will now be given. The waves described in this subsection were fairly regular and apparently steady over the time viewed. It is possible that long-term vacillation or other time-dependent behaviour existed but we have not yet searched for such phenomena. Three cases will be discussed: (1) slow rotation and moderate differential heating, (2) slow rotation and strong heating, and (3) moderately fast rotation with moderately strong heating.

Case 1 is for a rotation period of 10 s and a ΔT of 3.2 °C, which is near the upper part of the lower transition. A photo of the flow pattern is shown in figure 5(a). There are nine waves, with a slight irregularity of spacing which later became quite regular. The initial wavenumber observed was 13, and there was a gradual evolution to the nine-wave pattern (with individual waves weakening and dropping out). The waves fill the annulus width and lack any small-scale structure, and there is a definite spiral appearance, i.e., a westward phase shift with increasing radius.

Case 2 is shown in figure 5(b), which is for $\Omega = 45^\circ/\text{s}$ and $\Delta T = 15.8^\circ\text{C}$. This point is near the extreme upper transition curve. There are six regular waves, with a somewhat less spiral nature and with much sharper features than in Case 1. The initial wavenumber was 15, which was manifested by waves first appearing near the middle of the annulus.

Case 3 is shown in figure 4(b); here $\Omega = 90^\circ/\text{s}$ and $\Delta T = 10.5^\circ\text{C}$. This is the case described in the previous subsection, in which there were initially about 30 waves. The quasi-equilibrated pattern has eight waves with some irregularities (which were

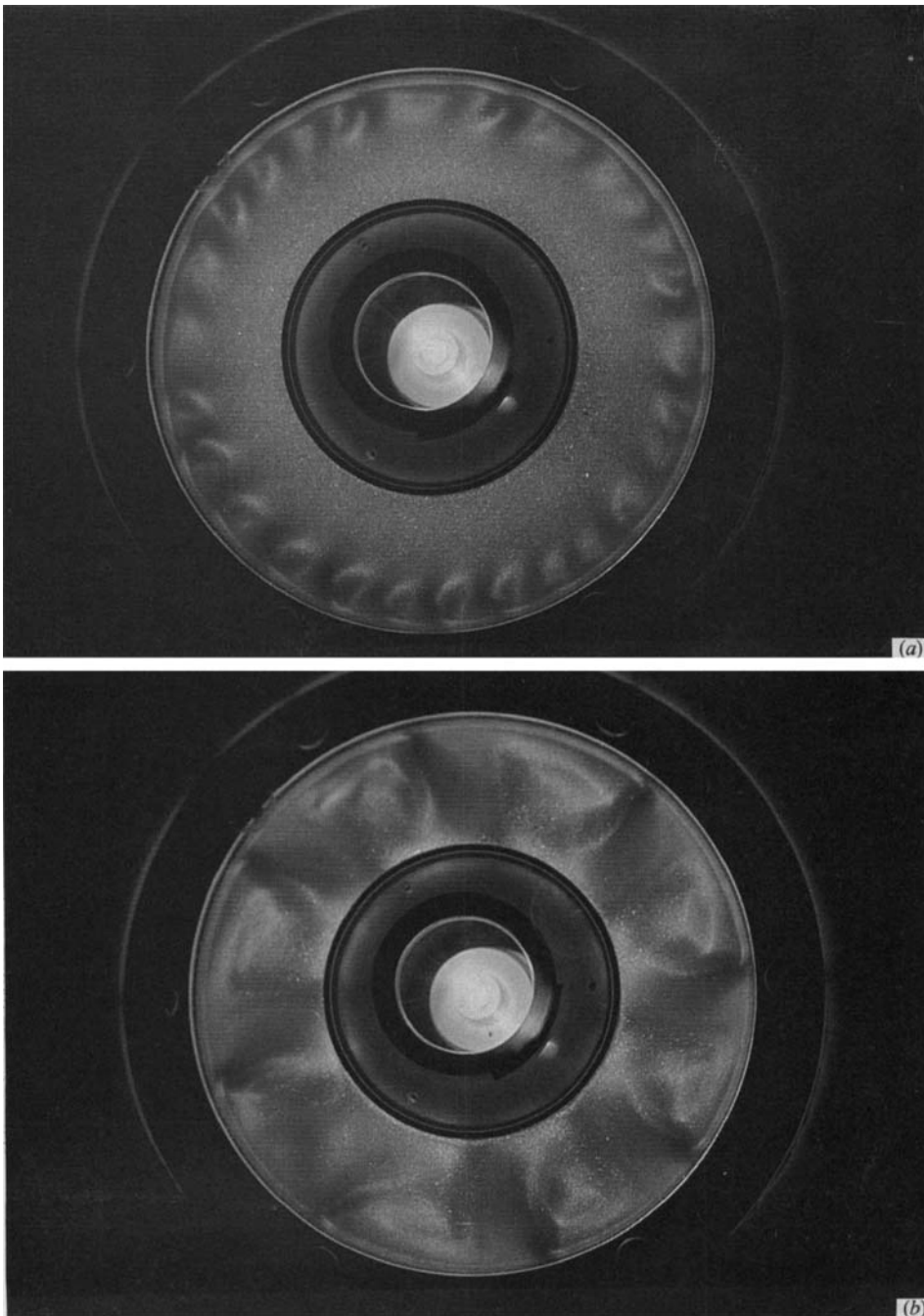


FIGURE 4. Photos of early waves (a) and equilibrated waves (b) for the case with $\Omega = 90^\circ/\text{s}$ and $\Delta T = 10.5^\circ\text{C}$ ($Ro = 0.011$, $Ta = 1.305 \times 10^6$).

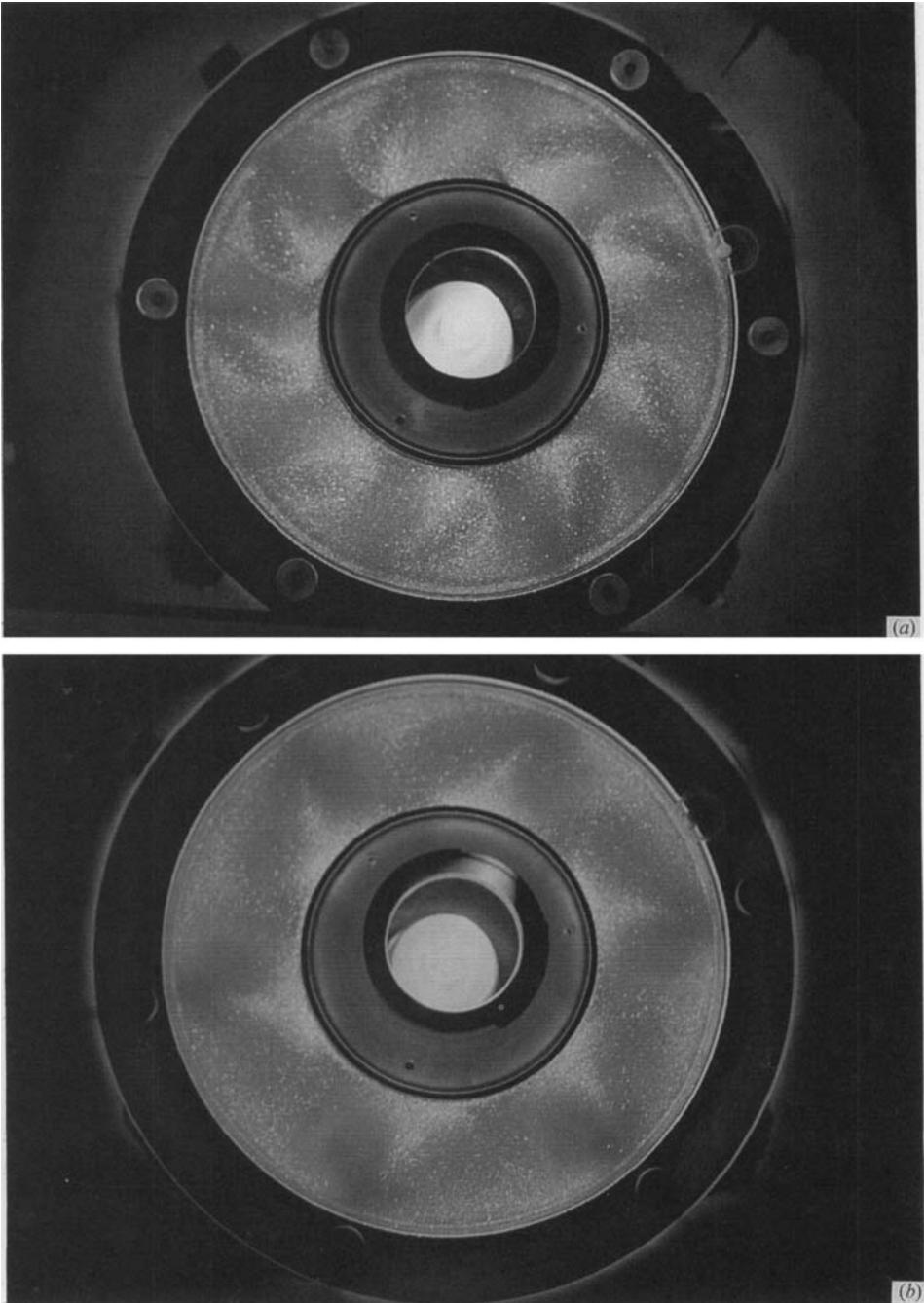


FIGURE 5. Photos of the equilibrated wave pattern for the cases (a) $\Omega = 36^\circ/\text{s}$ and $\Delta T = 3.2^\circ\text{C}$ ($Ro = 0.021$, $Ta = 2.09 \times 10^5$) and (b) $\Omega = 45^\circ/\text{s}$ and $\Delta T = 15.8^\circ\text{C}$ ($Ro = 0.065$, $Ta = 3.26 \times 10^5$).

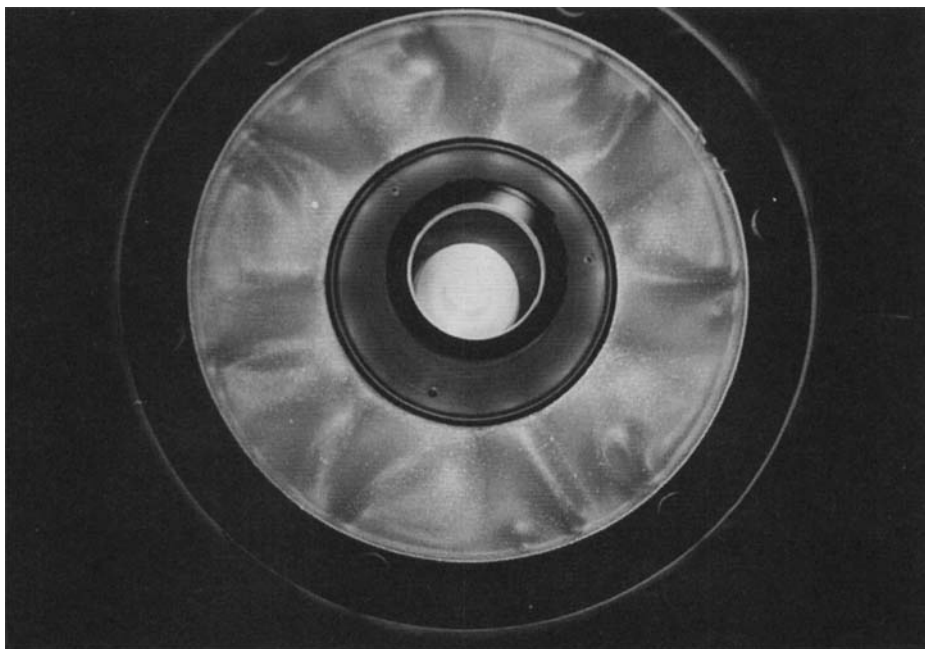


FIGURE 6. Photo of the quasi-equilibrated flow pattern for the case with $\Omega = 120^\circ/\text{s}$ and $\Delta T = 6.9^\circ\text{C}$ ($Ro = 0.0040$, $Ta = 2.32 \times 10^6$).

long-lived) and with some small-scale features, including sharp gradients in general. Despite the irregularities, it is clear that this flow is dominated by wavenumber 8. The flows described in the next sub-section are not so easily characterized.

4.4. *Irregular waves and propagating convection cells for large rotation and heating*

For strong heating and rotation, the flow pattern which eventually formed was irregular, with a mix of features that resulted in the inability of the observers to count a definite number of longitudinal waves. The transition to irregular flow was not sharp, with the onset of irregularity indicated by long-lived irregular spacing between waves and/or small-scale features which distorted the shape of the long waves. Often, 'double waves' appeared, which were apparently two long waves which were very close together and which remained so for as long as the flow was observed (≈ 1 hr). An example of a flow just inside the irregular regime is seen in figure 6, and a small-scale, transient feature is seen at about the 'five-o'clock' position, a short distance eastward of a long-lived, large-scale wave. This feature formed at the outer wall, later propagated inward to fill the annulus width, and eventually decayed. This type of phenomenon occurred for fast rotation and moderate to strong heating. We speculate that these are centrifugally induced buoyant convection cells.

5. Numerical results

5.1. *Transition to wave flow and structure of linear waves*

Since we obtained only flow pattern data from the experiments, the calculation of the transition curve and comparison with the laboratory results offers the most quantitative verification of the numerical and experimental procedures. The

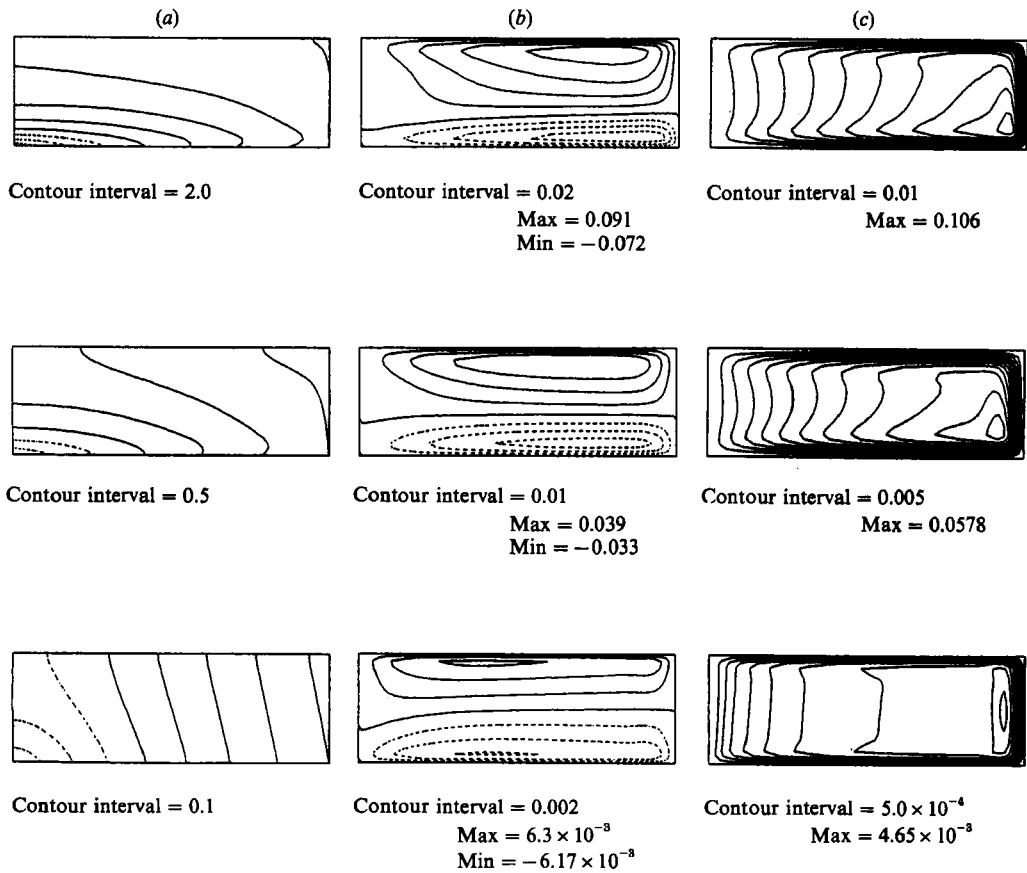


FIGURE 7. Steady axisymmetric solutions for three combinations of rotation rate and temperature difference. Upper row: $\Omega = 0.74 \text{ s}^{-1}$, $\Delta T = 15 \text{ }^\circ\text{C}$ ($Ro = 0.070$, $Ta = 2.90 \times 10^6$). Middle row: $\Omega = 0.46 \text{ s}^{-1}$, $\Delta T = 3 \text{ }^\circ\text{C}$ ($Ro = 0.036$, $Ta = 1.12 \times 10^6$). Lower row: $\Omega = 90^\circ/\text{s}$, $\Delta T = 0.8 \text{ }^\circ\text{C}$ ($Ro = 8.25 \times 10^{-4}$, $Ta = 1.305 \times 10^6$). (a) Temperature deviation from a reference value ($^\circ\text{C}$); (b) azimuthal velocity, positive for eastward flow (cm/s); and (c) stream function, the gradient of which is proportional and perpendicular to mass flux (circulation is counterclockwise, parallel to the contours). The outer (warm) wall is on the right. Dashed contours indicate negative values.

technique of numerically calculating the transition curve was to calculate a steady axisymmetric state for a given point in parameter space and then to calculate the set of linear waves with wavenumber near that observed experimentally to find the parameter values at which a wave first becomes unstable. The same technique and an earlier version of the computer code (before adding the capability of including wave-wave interactions) was used by Miller & Butler (1991) to calculate the transition curve for the conventional annulus of Fein (1973); excellent agreement with the experiments was obtained, especially in the case of the rigid-lid annulus. The calculated transition curve for the present annulus is shown in figure 2. It is seen that the upper part of the calculation curve is shifted downward in comparison with the experimental curve. Predicted wavenumbers and the calculated Taylor number at the knee agree very well with the experiments.

As previously noted, the experimental results were even farther from the numerical predictions than shown in figure 2 before more attention was paid to thermally insulating the apparatus from the surrounding air. Specifically, the lower

part of the laboratory curve (which was the only part completed before installing the additional insulation) was shifted further upward. The reason the results are still shifted may be related to imperfect temperature boundary conditions in the experiment. We suspect that the imperfections are a combination of non-zero heat fluxes through the Plexiglas lid and inner wall and other influences, which result in an effective temperature difference felt by the fluid that is somewhat smaller than that measured by the thermistors. Hignett *et al.* (1981) discussed the importance of ensuring zero heat flux through the upper lid, near which heat transport by the fluid flow is quite small. The temperature at the top of the flow cell can therefore be influenced by only a small heat flux through the plastic lid. This problem would indeed be more evident near the upper transition, where the interior static stability is more important in the transition. We wondered whether our measurement of the horizontal temperature difference on the lower surface might be inaccurate, but the thermistors were located very near the surface, and the isotherms within the copper plate must be very nearly vertical, based on heat flux calculations. A possibility is that the thin layer of Kalliroscope particles which settled on the surface inhibited the heat transfer enough to reduce the actual temperature difference. Another consideration was whether the thermal expansivity should be taken to be dependent upon the local temperature, but agreement was not improved by using a temperature-dependent thermal expansivity in the calculations. Although we have not been able to determine the reason for the systematic difference, we conclude that there is an imperfection in the experiment which reduces the effective temperature difference for large differential heating. Assuming that adjustments can be made in the external parameters to offset a systematic error, we proceed to use the numerical results to study the flow structure and underlying physics of the observed experimental results.

The structure of the steady axisymmetric flows for three points near the transition curve are shown in figure 7. These points are near the lower transition, the knee, and the upper transition. The temperature fields indicate that most of the heat enters the system through the outer wall, and the system is cooled by the inner part of the bottom surface. In the more highly convective cases (near the upper transition), the heating by the outer part of the lower surface is also significant. The azimuthal (eastward) wind consists of single jet structures near the top and bottom which are prograde and retrograde, respectively.

The wave structures (figures 8 and 9) corresponding to the axisymmetric fields discussed above can be compared with those of Miller & Gall (1983), who performed similar calculations for the conventional annulus. The structure of the waves for both configurations is fundamentally that of the Eady (1949) mode of baroclinic instability. There is a secondary maximum in wave vertical motion, but not in temperature, near the inner and outer walls. The latter fact differentiates the present structures from those of the conventional annulus studied by Miller & Gall, in which the temperature wave amplitude has maxima near the sidewalls. (However, it should be noted that the model of Miller & Gall assumed hydrostatic balance for the linear waves, an assumption that is not made here. The maxima near the sidewalls may not be so extreme when the hydrostatic assumption is not used.) Another aspect of the wave structures which is worth pointing out, and which may be seen in both the numerical and experimental results, is that for smaller rotation rates there is a substantial phase tilt westward for increasing radius, resulting in a spiral appearance. For higher rotation, this radial tilt is much smaller (compare figure 9 with figure 8). This aspect was noted by Miller & Fowles (1986), who performed experiments in an apparatus with a temperature gradient imposed upon both the upper and lower

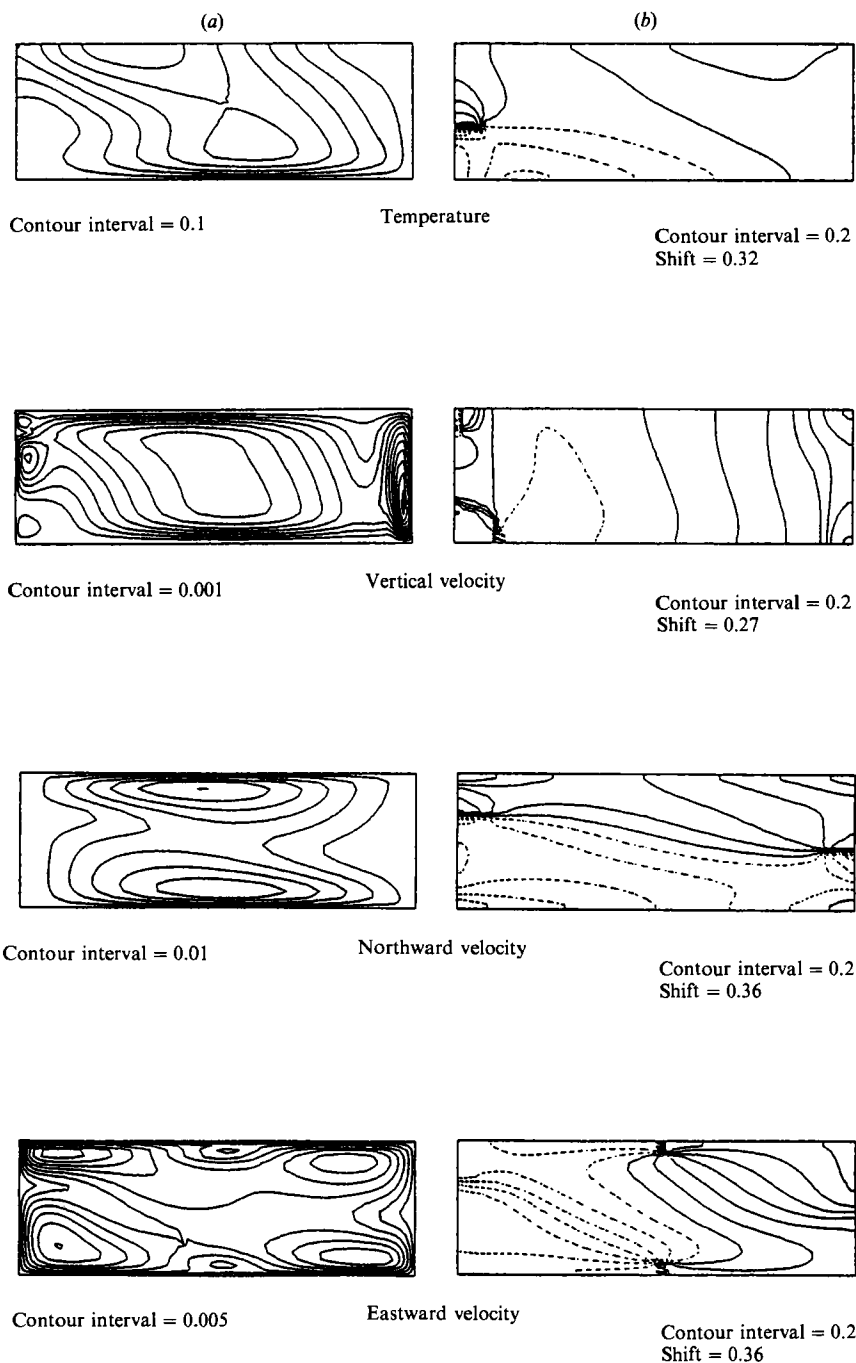


FIGURE 8. Fastest growing linear eigenmode components corresponding to the case shown in the upper row of figure 7. The wavenumber is 5. The wave is defined by (using temperature as an example): $T_k = \text{Re}(T_k e^{ikx})$, where T_k is a complex Fourier component and can be written as $|T_k|e^{i\theta}$. The quantities plotted are (a) $|T_k|$ (amplitude) and (b) θ (phase angle divided by π). The quantity 'shift' must be added to θ if the determination of relative phases between components is desired. Dashed contours indicate negative values; phase tilt is westward for increasing phase angle.

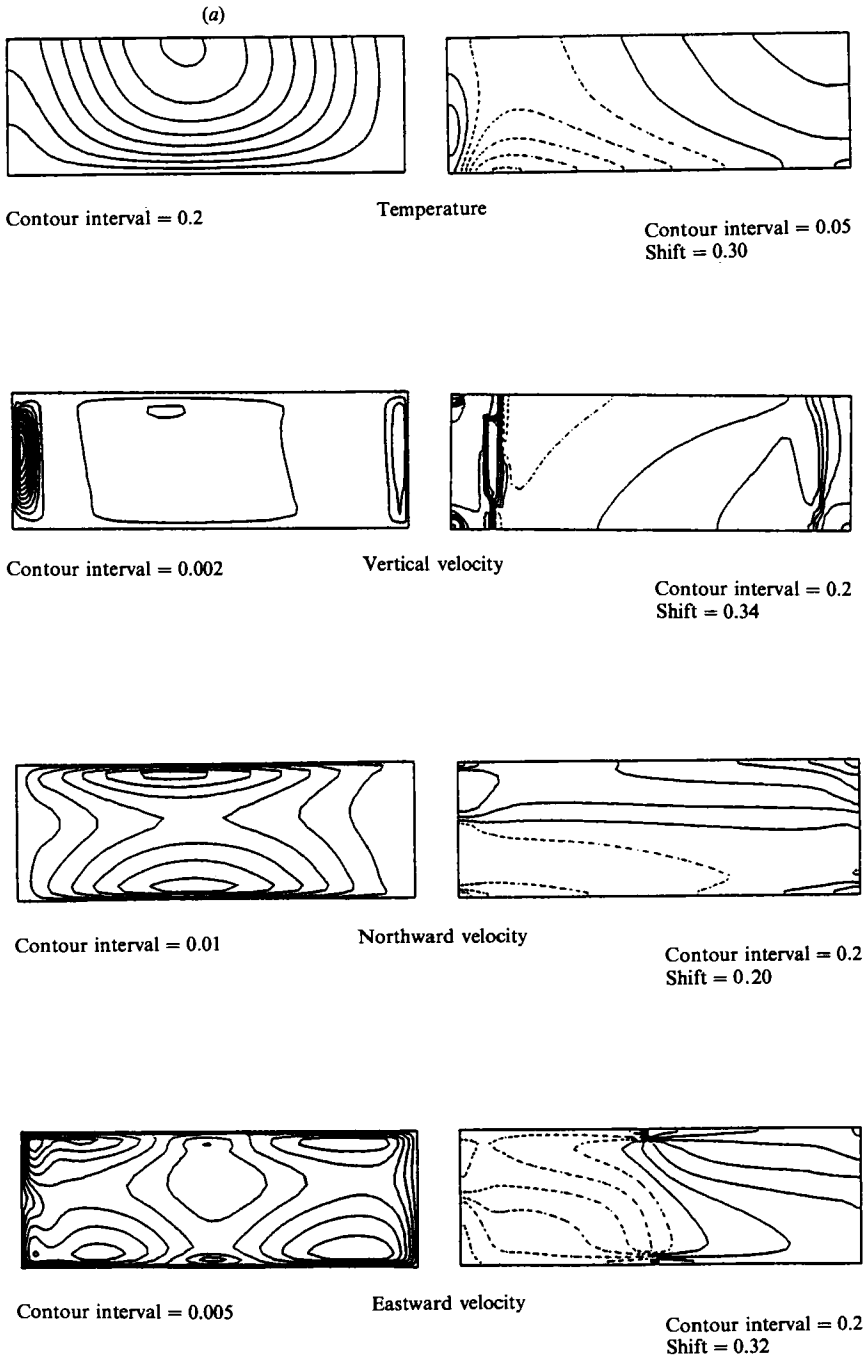


FIGURE 9. As in figure 8, but for the case shown in the lower row of figure 7.

surfaces, and who noted that the same spiral effect occurs for waves in a conventional annulus when the depth is small, relative to the width.

5.2. Evolution to longer waves and structure of the short-wave instabilities

The initial conditions used for all the time-dependent calculations were solid-body rotation and isothermal interior conditions (at the arithmetic mean temperature of the two lower corners), with the temperature gradient on the boundaries instantaneously applied at time zero. Since the viscosity of the working fluid (water) is nearly an order of magnitude larger than the thermal diffusivity, this approximates the initial conditions of the experiments. From the experimental results, there is a variety of wavenumber transitions which are of varying difficulty to model. For example, the transition from wavenumber N to $N-1$ would be fairly simple to model if wave-wave interactions were not important. If that were the case, then a limited number of waves (minimally, N and $N-1$) could be used. However, while a model run of this type may be able to qualitatively reproduce the experiment, one cannot be sure whether the result from such a calculation would be the same as one with fully nonlinear interactions included, or even whether a run without wave-wave interactions but with a broad range of waves would choose the same wavenumber as the experiment. Here, we give some results from both methods.

Calculations were performed for the case of $\Omega = 90^\circ/\text{s}$ and $\Delta T = 2^\circ\text{C}$. The experimental observation near this point was that the initial wavenumber was ten and the equilibrated wavenumber was eight. It is just above the lower transition curve, at $Ta = 1.3 \times 10^6$. Although details were somewhat different, the gross results in terms of initial and final wavenumber were nearly the same whether wave-wave interactions were included or not. Furthermore, the results resemble those of the experiment in the structure of the waves and in the fact that an irregular wavelength persisted for a very long period of time (the model was run for 136 min in fully nonlinear mode, wave numbers 1–20, and for 240 min with wavenumbers 7 to 12). Early in the fully nonlinear run, many waves, ranging from 8 to 13, had significant amplitude and an irregular 11-wave pattern was present in the total fields. (However, wavenumber 11 was not the largest-amplitude Fourier component.) A wavenumber 12 was first observed in the run lacking wave-wave interactions. At the end of the integration time, wavenumber 8 was dominating the run lacking full interactions, and wavenumbers 8 and 9 were still competing in the fully nonlinear run, with an irregular 9-wave pattern present in the fields. A time sequence of the fields from the fully nonlinear run indicated that the wavenumber transition process was due to individual waves weakening and merging with a nearby wave, as discussed in the description of the experiments. It should be noted that neither calculation was performed until true equilibration, although the flow in the case without wave-wave interactions seemed to have been settled on wavenumber 8 (i.e. others were small and still decaying). The final mean state in both cases has a double-jet structure in the zonal wind field, with much weaker thermal wind in the middle of the annulus than near the outer and inner regions.

The phenomenon of transition from initial short waves near the outer wall to long waves throughout the annulus was studied with the numerical model in fully nonlinear mode and with a wave factor of 5 for the particular case shown in figure 4. This set of calculations is not intended to reproduce all aspects of the experiments, which do not have such a 5-fold symmetry. The results do not include the very small-scale irregularity that occurs during the transition period, and the wavenumber predicted at the time the integration ended is 10. However, the major aspects of the

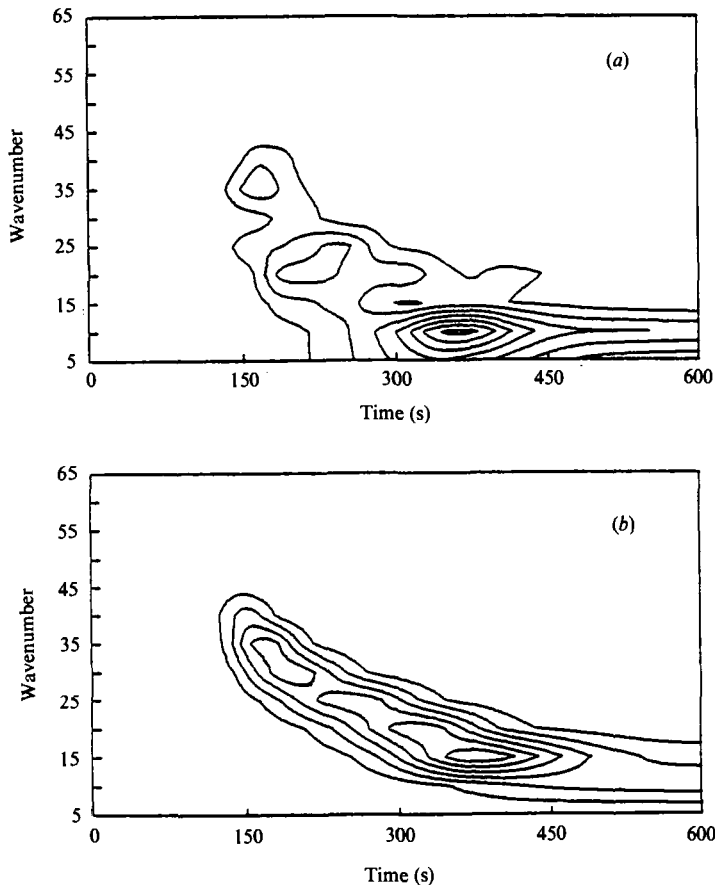


FIGURE 10. Evolution of kinetic energy spectrum with time for the case with $\Omega = 90^\circ/\text{s}$ and $\Delta T = 10^\circ\text{C}$ ($Ro = 0.010$, $Ta = 1.305 \times 10^9$): (a) the calculation with fully nonlinear interactions; (b) the calculation with wave-mean interactions but without wave-wave interactions. Both calculations were performed with waves 5, 10, ..., 95, 100 present.

transition described in the previous section can be simulated using this method. The evolution of the longitudinal wave spectrum in one of these integrations is shown in figure 10(a) (wavenumber 5, 10, ..., 100 were included in the calculations). The first wave which attains a significant amplitude is 35, which is in rough agreement with the experiments. Later, wave 25 becomes large and 35 is nearly gone; viewing an animation of the model results shows that this transition occurs through the disappearance of individual waves. Wave 10 is the next to dominate the spectrum, and it persisted until the end of the integration (which was for 10 min). As in the experiments, there was no indication that any of the long waves were 'parented' from any of the earlier, smaller waves.

Based upon both the experimental and the fully nonlinear numerical results from the case just discussed, an obvious question to ask is whether the wavenumber evolution involves wave-wave interaction, or whether it is simply competition among the waves for energy from the mean state. To address this question, another numerical integration was conducted on the above case, but with no wave-wave interactions and with the same waves included. These results are shown in figure 10(b). It is evident that the spectral evolution differs markedly from that of figure 10(a). The transition from wave 35 to wave 10 occurs in an unbroken stepwise sequence with

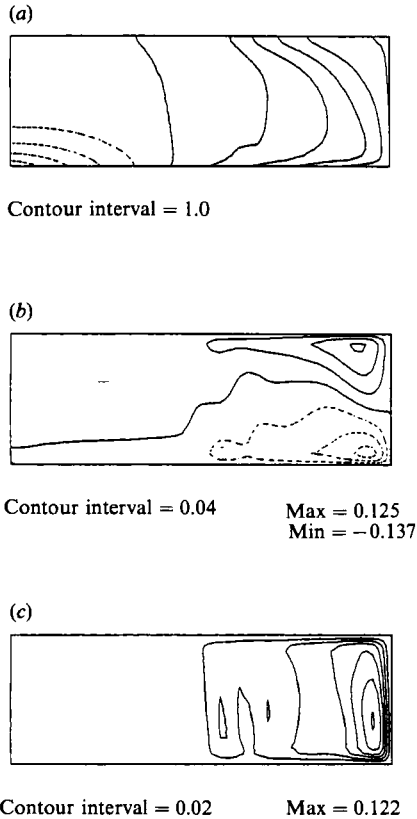


FIGURE 11. Azimuthal mean fields for the fully nonlinear calculation referenced in figure 10 120 s after the start of the calculation. See figure 7 for definitions, units, and contour scheme. (a) Temperature, (b) azimuthal velocity, (c) stream function.

every wave between 35 and 10 dominating for some period of time. These simulations clearly show that wave-wave interactions are important in the evolution of the longitudinal wave spectrum, although the initial and final dominant wavenumbers are nearly the same for the two calculations.

Of major interest is the character of the short waves that occur early in the experiment, i.e. whether they are of the Eady or Rayleigh-Bénard type. In order to elucidate the nature of the initial (short-wave) instability, plots of the longitudinal mean flow and dominant wave (number 35) after 2 min are shown in figures 11 and 12 for the fully nonlinear integration. The region containing the wave is approximately the position of strong horizontal temperature gradient, and the vertical gradient is positive (i.e. temperature increasing upward) in the upper two-thirds of the region containing the wave. Recall that initially the gradient was fully contained in the first grid interval from the boundaries, the interior being isothermal. In the vicinity of the wave, the fluid is initially heated from below and from the side. The flow is clearly acting to move the temperature gradient into the interior and to spread it throughout the volume. The structure of wave 35 is that of a baroclinic wave of limited radial extent, although there exists some radial structure in the amplitude plots. The (vertically) bimodal structure in radial velocity component, the westward phase tilt, and the phase relationships between temperature and velocity components are those of baroclinic waves. The vertical velocity component is smaller

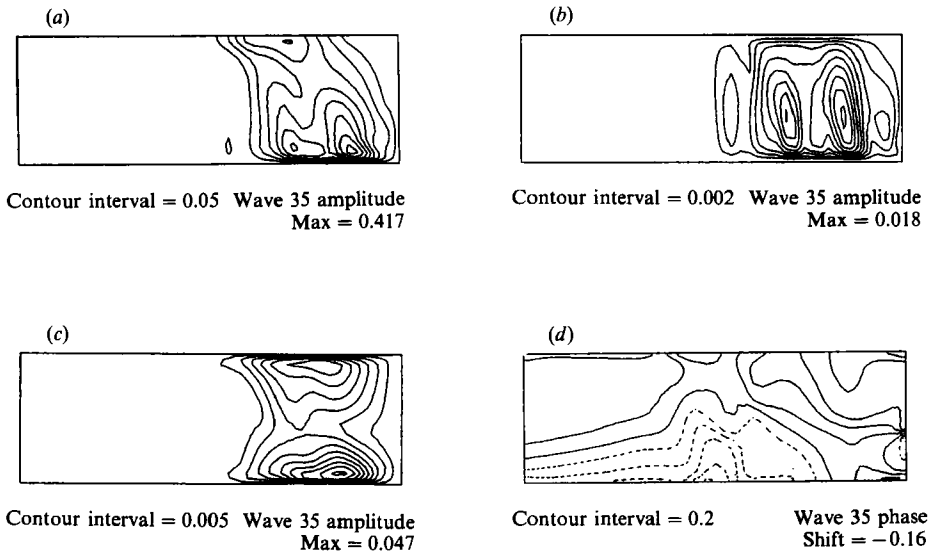


FIGURE 12. Wave number 35 components corresponding to figure 11. See figure 8 for definitions of quantities plotted. (a) Temperature, (b) vertical velocity, (c, d) northward velocity.

than the horizontal velocity, although it is of the same order of magnitude. The northward and vertical heat fluxes of the non-axisymmetric flow are of similar magnitude, although the vertical heat flux is the larger by about 10%. The total heat flux (upward and northward) of the axisymmetric flow is about $\frac{3}{4}$ of that of the wave flow, and the axisymmetric vertical heat flux is about 2.5 times larger than the axisymmetric northward heat flux.

5.3. Structure of the equilibrated 'long-wave' flow

The modelling of the equilibrated, regular long-wave flow is not as computationally demanding as the simulations of the evolution of the flow, since one can use the wavenumber observed in the experiment as a wave factor and include only a few harmonics of that wavenumber. As mentioned in the previous section, this would not test the model's ability to select the same wavenumber observed in the experiments. In this section we describe some results of long-term integrations, some of which were specified *a priori* to have the observed wavenumber, and in some of which the wavenumber was not specified.

We shall discuss the results of calculations for three cases: for the highest temperature difference used in the experiments (15 °C) and with rotation rates of 45°/s, 60°/s, and 90°/s. The slowest rotating case is for a rotation rate about 20% higher than that at the transition between axisymmetric and wave flow.

We discuss the 60°/s case first. We computed results using a broad range of wavenumbers (2, 4, ..., 24) and allowed the equilibrated wavenumber to be chosen by the model. The selected wavenumber was 8, which agrees with the experiments. Temperature, pressure, and vertical and horizontal velocities are shown in figure 13 for non-dimensional height = 0.206, which is just above the level of maximum temperature wave amplitude. The strong easterly flow near the outer wall is broken by the wave, where strong northward and southward flow interrupts the zonal wind. This north-south flow is in phase with the temperature field; i.e. the northward (southward) flow transports hot (cold) fluid. The flow slightly leads the temperature

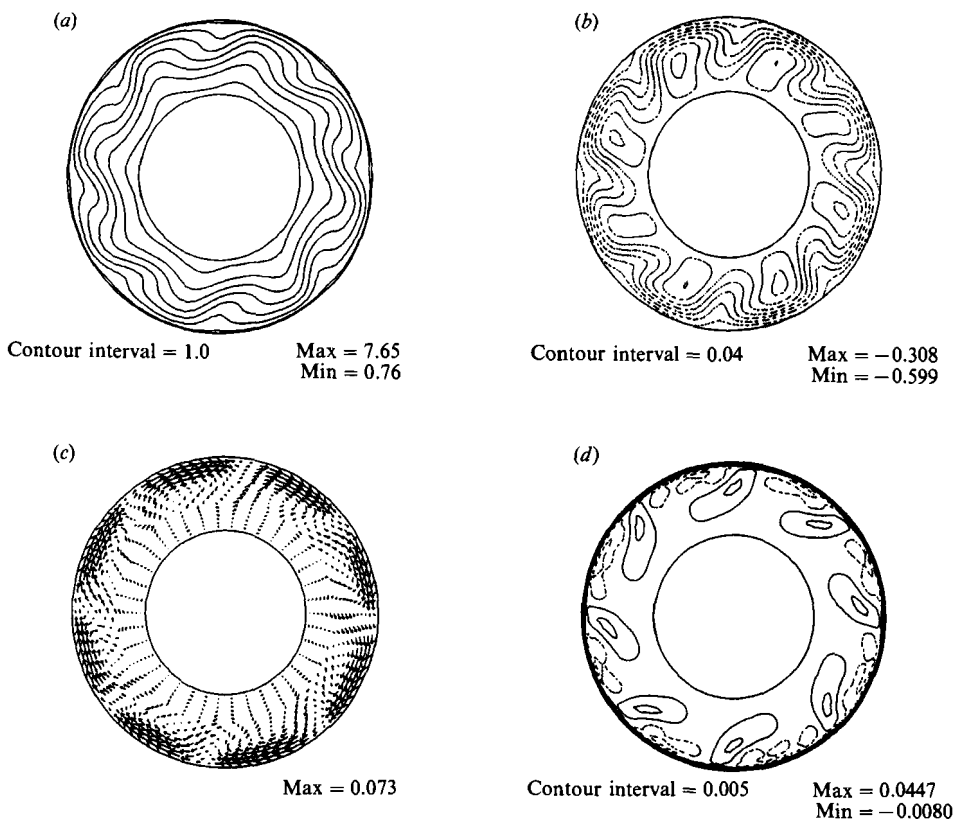


FIGURE 13. Plots of selected quantities for the equilibrated flow at height 0.412 cm for the fully nonlinear calculation (waves 2, 4, ..., 22, 24) for the case with $\Omega = 60^\circ/\text{s}$ and $\Delta T = 15^\circ\text{C}$ ($Ro = 0.035$, $Ta = 5.80 \times 10^6$). The quantity labelled 'pressure' is actually pressure deviation from hydrostatic, divided by a reference density, and temperature is deviation from a reference value ($^\circ\text{C}$). All units are c.g.s. (a) Temperature; (b) pressure; (c) horizontal velocity; (d) vertical velocity.

wave to result in eastward propagation. The wave structure is frontogenetical, i.e. there is a 'cold front' region of strong temperature gradient which is accompanied by low pressure, rising motion, and strong shear in the horizontal flow. The (interior) region of rising motion is much narrower than the general downward motion, as the coinciding region of warm fluid is narrower than that of the cold fluid, i.e. behind the cold front there is a broad region of cold, sinking fluid. Characteristic of the Eady instability, the vertical motion is apparently a response to the thermal field and not a cause of it, since the presence of stable stratification would tend to cause upward (downward) motion to be cooling (warming). The action of the wave in reducing the horizontal temperature gradient results in the vertical shear in the mean azimuthal velocity near two-thirds the distance from the inner to outer wall to be noticeably reduced from the steady axisymmetric field which was more nearly radially uniform. There is a double-jet structure, with strong jets in the corners near the outer wall and weaker jets near one-third the distance from the inner to outer wall (not shown).

In comparison with the above case, the more slowly rotating case (wavenumber 6, with harmonics 12 and 18, was specified) equilibrates with a much smaller amplitude wave and less of a frontal structure (though the asymmetry of the pressure highs and lows is still present). There is also less of an effect upon the mean azimuthal wind (i.e. no split jet structure).

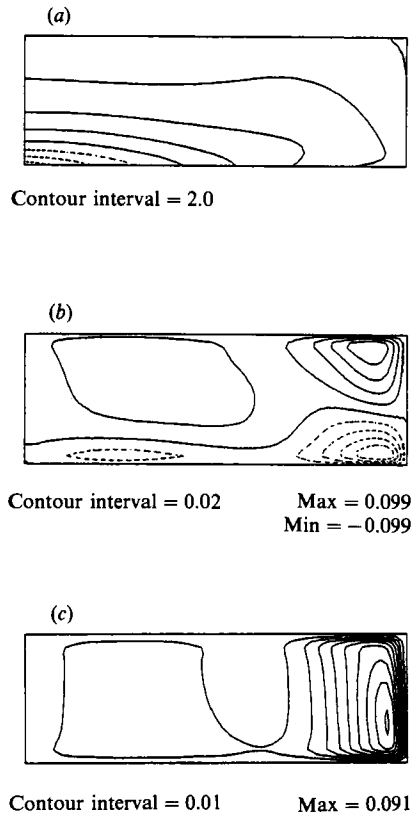


FIGURE 14. Equilibrated azimuthal mean fields for the fully nonlinear calculation, $\Omega = 90^\circ/\text{s}$ and $\Delta T = 15^\circ\text{C}$ ($Ro = 0.015$, $Ta = 1.305 \times 10^6$).

Like the moderate rotation case, the fastest-rotating case ($\Omega = 90^\circ/\text{s}$) was run in fully nonlinear mode, with waves 2 to 24 (wave factor of 2). Wavenumber 6 was selected by the model, a longer wave than the $60^\circ/\text{s}$ case which is in agreement with the experiments (wave 7 was observed). Nonlinear aspects, including frontal features and feedback to the mean flow, are the strongest of the three cases. The shear of the horizontal flow is strong and confined to the region of the cold front, consistent with the pattern observed in the experiments. The mean horizontal temperature gradient is actually reversed in the interior, where there is virtually no vertical shear of the azimuthal wind and there is a Ferrell cell – a region with rising motion north of sinking motion (figure 14).

6. Summary and concluding comments

A gross description of the flow characteristics of a rotating, thermally driven cylindrical annulus with the horizontal gradient imposed upon the lower horizontal surface has been given, in terms of both laboratory experiments and numerical calculations. The vertical depth is about one-third the radial width. The transition diagram, in thermal Rossby number–Taylor number space, between axisymmetric and wave flow has been determined, and it is shown that the shape of this curve is similar to that of the conventional, side-heated and -cooled baroclinic annulus. Agreement in the transition curve between numerical calculations and the

experiments is fairly good, although there is noticeable discrepancy in determining the upper transition. Agreement in predicting wavenumbers, both near the transition and within the wave regime, is very good. Away from the transition curve and within the wave regime, there is an evolution from larger to smaller wavenumbers as the flow equilibrates, which is well captured by the numerical model for those cases studied. (Modelling the cases of irregular flow was not attempted.) Far enough into the wave regime, the initial waves are of small scale both in longitude and in latitude (radius), and they form near the outer wall and subsequently grow inward, decreasing in number as the slower-growing waves give way to the more vigorous ones. The numerical studies indicate that these waves are active in a region with strong horizontal temperature gradient and with positive vertical stratification through most of the depth. There is a period of irregular flow before a transition to an equilibrated long-wave state. The equilibrated wavenumber is not a simple monotonic function of any of the external parameters, although it is smallest near the upper transition curve and usually increases with decreasing temperature difference. The structure of the equilibrated waves includes a horizontal tilt from southwest to northeast which decreases with increasing rotation. As in the conventional annulus, the equilibrated flow becomes spatially irregular for large enough Taylor number and differential heating. For rapid enough rotation and large enough heating, small-scale features appear which continually form near the outer wall and propagate inward before merging with the larger-scale flow. It is speculated that these latter features are centrifugally induced buoyant plumes.

Miller & Fowles (1986) and Hathaway & Fowles (1986) found that the system with the horizontal gradient imposed upon both horizontal surfaces has a regime diagram which does not have an upper symmetric regime. This finding was also the case in the numerical study of Miller & Fehribach (1990) for a similar spherical system. The primary reason cited for this finding was that the horizontal conducting boundaries prevent the interior static stability from indefinitely increasing as the thermal forcing is increased. While the thermal advection certainly strengthens with the Hadley circulation, there is a statically unstable region near the horizontal boundaries in those systems, which allows the waves to grow. In the present system, where only the lower horizontal surface is thermally conducting, there is indeed a statically unstable region for strong thermal forcing above the lower boundary near the outer wall. However, the presence of the thermally conducting outer wall prevents this region from becoming large enough to preclude the upper symmetric regime.

A motivation for studying the present system was the expectation that it would be more like the Earth's atmosphere than the side-heated and -cooled system in the sense that the sidewalls would have less influence on the flow. As discussed by Miller & Gall (1983), the sidewalls have a strong effect on the transition between wave flow and axisymmetric flow in the conventional annulus, at least when the vertical depth is not thin, relative to the annulus width. One reason for this importance is that when both horizontal surfaces are thermal insulators the isotherms are free to be advected by the Hadley circulation, which results in the temperature gradient being pushed into the corners (upper-inner and lower-outer). Eddy vertical velocity in the corner regions is significant in the energy conversion process, and thermal and mechanical dissipation of the eddies is also important there.

In addition, the prediction of the transition from axisymmetric flow to baroclinic waves by quasi-geostrophic theory is much better for the new annulus than for the conventional annulus, at least for the usual case in which the vertical/horizontal aspect ratio for the latter system is of order one or greater. The tall vertical height

results in the internal isothermal slope being greater than one (i.e. closer to vertical than to horizontal) for most of parameter space, a violation of an assumption of the quasi-geostrophic theory of Barcilon (1964). Our expectation was fulfilled that the present system would be better predicted by the simple quasi-geostrophic theory of Barcilon (as extended by Hide, 1969 for arbitrary aspect ratio) than for the conventional annulus studies by Miller & Gall (1983). To be specific, the isothermal slope in the centre of the annulus near the knee of the transition curve is about 0.4 for the present system, which gives a prediction of the critical Ta of 1.7×10^4 , in comparison with the experimental and numerical value of 1×10^5 . While a factor of 6 is not a very good quantitative prediction, it is better than the comparison for the square, conventional annulus cited by Miller & Gall (1983), in which the difference between theory and numerical results was a factor of 50. Comparisons of numerical calculations with the theoretical predictions lead to the conclusion that the improvement is due to three effects, which when added to the Miller & Gall case give increasingly better comparisons with the theory. The first effect is the use of a no-slip upper boundary, which increases the Ekman flow and hence the basic-state thermal advection at the top of the flow cell. The second effect is the height/width aspect ratio. Numerical calculations were made for a side-heated and -cooled annulus with no-slip boundaries and with the same geometry as the present, new annulus. In that case, the numerically determined isothermal slope near the knee is about 0.58, and the theoretically predicted Ta is about 13 times smaller than the numerical result. The third effect is of course the thermal boundary conditions of the new annulus. For the present geometry, the theory predicts the critical wavenumber near the knee to be 5 (this result is not dependent on the isothermal slope). This prediction is actually better for the side-heated and -cooled case, in which the numerical model predicts 6, than for the new annulus (wavenumber 9). The theoretical prediction of the internal Brunt-Väisälä frequency at the knee is very good for the present geometry with both boundary temperature configurations.

Future work with this system will investigate whether there exists interesting long-term time-dependent behaviour such as vacillation, and whether the numerical model agrees with quantitative measurements of wave amplitude. Experiments will be performed with the apparatus instrumented with thermistors to measure the temperature at an array of points on the upper lid of the apparatus, giving a quantitative measure of the amplitude and phase propagation of the waves while minimally interfering with the flow. This work should increase the applicability of the experiments to geophysical situations and allow further comparisons with the side-heated and -cooled experiments.

The authors are most grateful for the contribution of Mr Oscar Holderer, who constructed the apparatus and greatly assisted in its design. Drs Dan Fitzjarrald and Fred Leslie also contributed toward the design of the apparatus, and it was Dr Fitzjarrald who suggested the use of a laser for visualization. The support and encouragement of Dr George Fichtl is gratefully acknowledged. This research was supported by the Office of Space Science and Applications, Global Scale Processes Research Program, at NASA Headquarters.

REFERENCES

- BARCLON, V. 1964 Role of the Ekman layers in the stability of the symmetric regime obtained in a rotating annulus. *J. Atmos. Sci.* **21**, 219–299.
- BUZYNA, G., PFEFFER, R. L. & KUNG, R. 1989 Kinematic properties of wave amplitude vacillation in a thermally driven rotating fluid. *J. Atmos. Sci.* **46**, 2716–2729.
- EADY, E. T. 1949 Long waves and cyclone waves. *Tellus* **1**, 35–52.
- FEIN, J. S. 1973 An experimental study of the effects of the upper boundary condition on the thermal convection in a rotating, differentially heated cylindrical annulus of water. *Geophys. Fluid Dyn.* **5**, 213–248.
- FOWLIS, W. W. & HIDE, R. 1965 Thermal convection in a rotating annulus of liquid: Effect of viscosity on the transition between axisymmetric and nonaxisymmetric flow regimes. *J. Atmos. Sci.* **22**, 541–558.
- HATHAWAY, D. H. & FOWLIS, W. W. 1986 Flow regimes in a shallow rotating cylindrical annulus with temperature gradients imposed on the horizontal boundaries. *J. Fluid Mech.* **172**, 401–418.
- HIDE, R. 1969 Some laboratory experiments on free thermal convection in a rotating fluid subject to a horizontal temperature gradient and their relation to the theory of the global atmospheric circulation. In *The Global Circulation of the Atmosphere* (ed. G. A. Corby), pp. 196–221. London: Royal Meteorological Society.
- HIDE, R. & MASON, P. J. 1975 Sloping convection in a rotating fluid. *Adv. Geophys.* **24**, 47–100.
- HIGNETT, P., IBBETSON, A. & KILLWORTH, P. D. 1981 On rotating thermal convection driven by non-uniform heating from below. *J. Fluid Mech.* **109**, 161–187.
- JAMES, I. N. & HOSKINS, B. J. 1985 Some comparisons of atmospheric internal and boundary baroclinic instability. *J. Atmos. Sci.* **42**, 2142–2155.
- KOSCHMEIDER, E. L. & LEWIS, E. R. 1986 Hadley circulations on a nonuniformly heating rotating plate. *J. Atmos. Sci.* **43**, 2514–2526.
- MILLER, T. L. & BUTLER, K. A. 1991 Hysteresis and the transition between axisymmetric flow and wave flow in the baroclinic annulus. *J. Atmos. Sci.* **48**, 811–823.
- MILLER, T. L. & FEHRIBACH, J. D. 1990 A numerical study of the onset of baroclinic instabilities in spherical geometry. *Geophys. Astrophys. Fluid Dyn.* **52**, 25–43.
- MILLER, T. L. & FOWLIS, W. W. 1986 Laboratory experiments in a baroclinic annulus with heating and cooling on the horizontal boundaries. *Geophys. Astrophys. Fluid Dyn.* **34**, 283–300.
- MILLER, T. L. & GALL, R. L. 1983 A linear analysis of the transition curve for the baroclinic annulus. *J. Atmos. Sci.* **40**, 2293–2303.
- MILLER, T. L., LU, H.-I. & BUTLER, K. A. 1991 A fully nonlinear, mixed spectral and finite difference model for thermally-driven, rotating flow. *J. Comput. Phys.* (submitted).